NMR Paramagnetic Relaxation Enhancement: ZFS-Limit Behavior for $S = 3/2$

J. C. Miller, S. M. Abernathy, L. L. Lohr, and R. R. Sharp*

The Department of Chemistry, The University of Michigan, Ann Arbor, Michigan 48109

Received: May 3, 2000; In Final Form: August 8, 2000

The NMR paramagnetic relaxation enhancement (NMR-PRE) induced by transition metal ions with electron spin $S = 1$ is strongly influenced by zero-field splitting (ZFS) interactions when the ZFS Hamiltonian is comparable or greater in magnitude than the electronic Zeeman Hamiltonian ($H_{ZFS} \geq H_{Zeem}$). In the vicinity of the ZFS limit ($H_{ZFS} \gg H_{Zeem}$), the spatial quantization of the electron spin motion is oriented along the molecule-fixed principal axes of the ZFS tensor. In this situation, the NMR-PRE, corrected to constant electron−nuclear interspin distance, has been predicted to be a function of the orientation of the electron−nuclear interspin vector with respect to the principal axes of the molecular frame. This prediction was tested experimentally and confirmed for $S = {}^3/_2$ using the complex, $Co^{II}(acac)_2(H_2O)_2$, for which the ZFS-limit axial/equatorial T_1 ratio, $\rho = 2.7 \pm 0.4$, is substantially greater than the Zeeman limit value of unity. A second theoretical prediction has been tested concerning characteristic differences in the effect of ZFS rhombicity on the magnetic field profile of the NMR-PRE produced by integer and half-integer spins. For $S = 1$, the ZFS-limit NMR-PRE is profoundly depressed due to the effects of the orthorhombic terms of the ZFS tensor, a phenomenon which results physically from the splitting of the $|\pm 1\rangle$ non-Kramers doublet by ZFS rhombicity and consequent alterations in the spin eigenfunctions. This depression is reversed by the application of a Zeeman field when the Zeeman energy exceeds the $|\pm 1\rangle$ doublet splitting produced by ZFS rhombicity. Thus, the NMR-PRE of orthorhombic $S = 1$ Ni(II) complexes exhibits a characteristic dispersive feature in which the NMR relaxation efficiency increases several-fold between about 0.2 and 10 T. For half-integer spins, this phenomenon is expected not to be present because the Kramers doublets remain unsplit by ZFS interactions of any magnitude or symmetry. This prediction was tested and confirmed through measurements of the magnetic field dependence of the NMR-PRE produced by the $S = {}^3/_2$ complex, $Co^{II}(acac)_2(H_2O)_2$, the NMR-PRE behavior of which differed qualitatively from that of the analogous $S = 1$ complex, $Ni^{II}(acac)_2(H_2O)_2$, as well as from other previously studied $S = 1$ model compounds.

Introduction

The introduction of small concentrations of paramagnetic species in solution enhances the relaxation rates of nuclear spins on ligand and solvent species, a phenomenon called the NMR-paramagnetic relaxation enhancement (NMR-PRE). For paramagnetic solutes with $S \geq 1$, the NMR-PRE is strongly influenced by the zero-field splitting (ZFS) interaction at Zeeman field strengths where the ZFS Hamiltonian is comparable to or greater than the electronic Zeeman Hamiltonian ($H_{ZFS} \geq H_{Zeem}$). The ZFS interaction, which results from an interplay of the spin and orbital angular momenta mediated by the crystal field, vanishes for $S = {}^1/_2$ but is present for $S \geq 1$ unless precluded by reasons of symmetry of the metal ion; the quadratic ZFS interaction vanishes in cubic or higher site symmetry. Over the past decade, a considerable body of theoretical work from this[1−11] and other[12−21] laboratories has been directed toward incorporating the effects of the ZFS interaction into the theory of the NMR-PRE.

In the vicinity of the ZFS limit ($H_{ZFS} \gg H_{Zeem}$), the motion of the electron spin is driven by the ZFS Hamiltonian, and as a result, the electron spin motion is spatially quantized (or polarized) along the molecule-fixed principal axes of the ZFS tensor rather than along the Zeeman field. In this situation, the mean-square local dipolar field of the electron spin differs at axial and equatorial positions with respect to the ZFS tensor. For $S = 1$, the ZFS limit NMR-PRE, corrected to constant electron−nuclear interspin distance, has been predicted[1,3,5] to be up to 4-fold greater for axial nuclear positions than for equatorial positions; i.e., the axial/equatorial T_{1p}^{-1} ratio, ρ, is thus predicted to lie in the range $1 \leq \rho \leq 4$, where, in comparison, the Zeeman limit value is unity.[22−23] This prediction has been confirmed experimentally.[24] Angular dependence in R_{1p} is also expected for $S = {}^3/_2$, although the physical situation is rather different than that for $S = 1$. We report here an analysis of the $S = {}^3/_2$ case and an experimental measurement of the molecular frame angular dependence of R_{1p} for the $S = {}^3/_2$ complex, $Co^{II}(acac)_2(H_2O)_2$. The measured ZFS-limit ratio, $\rho = 2.7 \pm 0.4$, is consistent with theoretical analysis.

A second theoretical prediction[6−8,25] has also been tested concerning characteristic differences in the effect of ZFS rhombicity on the magnetic field profile of the NMR-PRE produced by $S = 1$ vs $S = {}^3/_2$. For $S = 1$, the NMR-PRE is profoundly depressed in the ZFS limit due to effects of the orthorhombic components of the ZFS tensor, which split the $|\pm 1\rangle$ non-Kramers doublet, forcing a Cartesian polarization on the spin eigenfunctions. In the orthorhombic ZFS limit, the diagonal part of $\langle S_z \rangle$, evaluated in the spin eigenbasis, vanishes, and in consequence, the NMR-PRE is suppressed, often several-fold, relative to the value calculated for a cylindrical ZFS tensor. The rhombicity-induced ZFS-limit depression in the NMR-PRE is reversed by the application of a Zeeman field when the

* Corresponding author. E-mail: rrsharp@umich.edu. Fax: (734)-647−4865.

10.1021/jp001685s CCC: $19.00
Published on Web 09/26/2000

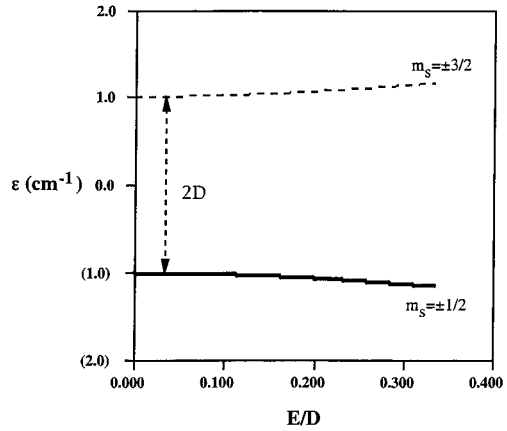

Figure 1. Spin energy level diagram for $S = {}^3/_2$ in a powder sample when the Zeeman field is zero. ZFS rhombicity (E/D) is plotted on the abscissa.

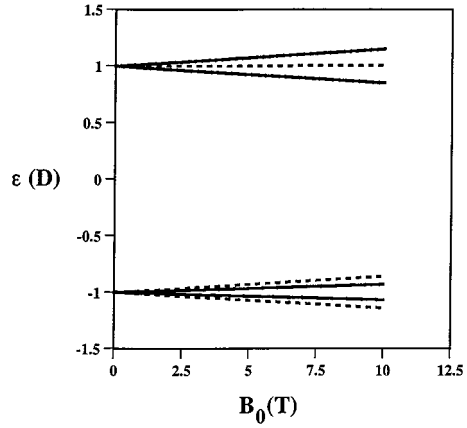

Figure 2. Spin energy level diagram for $S = {}^3/_2$ with a cylindrical ZFS tensor ($E/D = 0$) as a function of Zeeman field strength in a powder sample.

Zeeman energy rises above the $|\pm 1\rangle$ doublet splitting. Experimental results have confirmed this phenomenon. The NMR-PRE of orthorhombic $S = 1$ Ni(II) complexes exhibits a characteristic dispersive feature in which the NMR relaxation efficiency increases several-fold between about 0.2 and 10 T; this feature is, as predicted,[26] absent in the D_{3d} complex $Ni^{II}(en)_3$.

For half-integer spins, an analogous dispersive feature is expected to be absent because the Kramers doublets remain unsplit by ZFS interactions of any magnitude or symmetry, and there is no corresponding rhombicity-induced change in the spin eigenfunctions. We report here the results of an experimental test of this prediction that is based on a measurement of the T_1 magnetic field dispersion profile produced by the orthorhombic $S = {}^3/_2$ complex, $Co^{II}(acac)_2(H_2O)_2$. As predicted, the NMR-PRE behavior of this complex differs qualitatively from that of the analogous $S = 1$ complex, $Ni^{II}(acac)_2(H_2O)_2$, as well as from other previously studied $S = 1$ orthorhombic Ni(II) complexes.[26]

Theory

The ZFS limit spin level diagram for $S = {}^3/_2$ is shown in Figure 1. There are two Kramers doublets, $|\pm {}^1/_2\rangle$ and $|\pm {}^3/_2\rangle$, which are not split by the ZFS interaction in the absence of a Zeeman field. The ZFS splitting is 2D in a uniaxial ZFS field. ZFS rhombicity ($E \neq 0$) mixes the spin states for which $\Delta m_S = \pm 2$; thus, the rhombic ZFS term mixes the $|+{}^3/_2\rangle$ state with the $|-{}^1/_2\rangle$ state and $|-{}^3/_2\rangle$ with $|+{}^1/_2\rangle$. This mixing increases the *inter*doublet separation but, in the absence of a Zeeman field, does not break the degeneracy of the Kramers doublets. Figure 2 shows the level diagram for $S = {}^3/_2$ with a cylindrical ZFS tensor ($E = 0$) as a function of Zeeman field strength in a powder sample. The Zeeman field splits the Kramers doublets by an amount which depends on the angle between the axis (z) of the applied magnetic field and the molecule-fixed principal axis ($\hat{z}$) of the ZFS tensor. In the presence of a Zeeman field, the spin levels in a randomly oriented sample broaden into a band structure.

For octahedral Co(II), the ZFS splitting is very large,[27] approximately 160 cm^{-1} in $Co^{II}(acac)_2(H_2O)_2$, and positive so that the $|\pm {}^3/_2\rangle$ doublet is above the $|\pm {}^1/_2\rangle$ doublet. The Kramers doublets are well separated in energy and must be treated separately. As is shown below, the electron spin relaxation properties are very different within the two doublet manifolds, such that $\tau_{S,\pm 3/2} \approx 2$ ps for the $|\pm {}^3/_2\rangle$ doublet and $\tau_{S,\pm 1/2} \approx 0.2$ ps for the $|\pm {}^1/_2\rangle$ doublet.

Computations were carried out using the computer program RotJmpDyn.f,[28] which implements theory at several levels: (1) the Zeeman limit (SBM) theory;[22,23,29] (2) the theory of ref 11, which gives closed-form expressions that parallel the Zeeman limit expressions but are valid in the slow-reorientation orthorhombic ZFS limit; (3) slow-reorientation theory with arbitrary magnitudes of the ZFS and Zeeman Hamiltonians; (4) spin dynamics simulations,[7,28] which generalize level 3 to incorporate the effects of Brownian reorientation. Level 3, rather than SD simulations, was used in computations because this level accommodates the incorporation of level-specific electron spin relaxation times, as described above. Slow reorientation is amply satisfied by the chemical system; an estimate of $\tau_R^{(2)}$ from Debye's theory[31] gives a reorientational correlational time $\tau_R^{(2)} \approx 80$ ps at 20 °C for $Co^{II}(acac)_2(H_2O)_2$ in water.

For the purpose of analyzing the physics of the relaxation mechanism, the closed-form expressions of level 2 are useful. In this approximation, the NMR T_1 paramagnetic relaxation rate, R_{1p}, can be written as a sum of molecular frame Cartesian components,

$$R_{1p} = R_{1\hat{x}} + R_{1\hat{y}} + R_{1\hat{y}} \tag{1a}$$

$$R_{1\hat{r}} = (8/3)(\gamma_I g_e \beta_e)^2 \left(\frac{\mu_o}{4\pi}\right)^2 r_{IS}^{-6}[1 + P_2(\cos\theta_{\hat{r}})] \times \sum_{\mu,\nu} P_\mu^o |\langle\mu|S_{\hat{r}}|\nu\rangle|^2 J_{\hat{r}}(\omega_{\mu,\nu} + \omega_I) \tag{1b}$$

$$(\hat{r} = \hat{x}, \hat{y}, \hat{z})$$

where γ_I is the nuclear gyromagnetic ratio, β_e is the Bohr magneton, and μ_0 is the permeability of free space. The electron g-factor, g_e, may in general depend on the Kramers doublet (μ), and it may be anisotropic. We show below that g-values which differ for the two Kramers doublets but are isotropic within each doublet are appropriate for Co(II) in NMR-PRE theory. Thus we use level-specific g-values, $g_e^{(\pm 3/2)}$ and $g_e^{(\pm 1/2)}$. Equation 1a is expressed in the molecule-fixed coordinate frame ($\hat{x}$, $\hat{y}$, $\hat{z}$) of the ZFS-PAS (the laboratory coordinate frame is denoted (x, y, z)). The interspin distance is r_{IS}, and $\cos\theta_{\hat{r}}$ is the direction cosine of the interspin vector with respect to the $\hat{r}$th coordinate axis. The sum is over eigenstates $\{\mu,\nu\}$ of S, and the spin operators are expressed in the molecular frame. P_μ^o is the fractional Boltzmann population of the eigenstate $|\mu\rangle$. $J_{\hat{r}}(\omega)$ are dipolar power density functions,

$$J_{\hat{r}}(\omega) = \frac{\tau_S}{1 + \omega^2 {\tau_S}^2} \quad (1c)$$

where τ_S is electron spin relaxation time.

Uniaxial ZFS Limit. In the uniaxial ZFS limit, eq 1b can be simplified as follows. The matrix of $\langle S_{\hat{z}} \rangle$ is diagonal with elements equal to m_S. Thus, for $R_{1\hat{z}}$, the nonvanishing terms have $\omega_{\mu,\nu} = 0$, giving

$$R_{1\hat{z}} = (8/3)(\gamma_I \beta_e)^2 \left(\frac{\mu_o}{4\pi}\right)^2 {r_{IS}}^{-6} [1 + P_2(\cos\theta_{\hat{z}})]((9/2)$$
$$[g_e^{(\pm 3/2)}]^2 P^o_{3/2} J^{(\pm 3/2)}_{\hat{z}}(\omega_I) + (1/2)[g_e^{(\pm 1/2)}]^2 P^o_{1/2} J^{(\pm 1/2)}_{\hat{z}}(\omega_I)) \quad (2a)$$

Electron spin relaxation times within the two Kramers doublets are substantially different, so the spectral density functions are denoted $(\pm^1/_2)$ and $(\pm^3/_2)$.

In the uniaxial ZFS limit, we write $R_{1\hat{\perp}}$ for the transverse contribution. Nonvanishing matrix elements of $\langle S_{\hat{x}} \rangle$ and $\langle S_{\hat{y}} \rangle$ couple the 1Q transitions, $\{\pm^3/_2 \leftrightarrow \pm^1/_2\}$ and $\{+^1/_2 \leftrightarrow -^1/_2\}$, for which the ZFS-limit transition frequencies are $\omega = 2\omega_D$ (*inter*doublet) and $\omega = 0$ (*intra*doublet), respectively. The *inter*doublet transition frequencies are very high, about 160 cm^{-1} for orthorhombic Co(II)[27] and $2\omega_D\tau_S \gg 1$. The relaxation contributions of these terms are negligible. However, the $\{+^1/_2 \leftrightarrow -^1/_2\}$ *intra*doublet $R_{1\hat{\perp}}$ contribution is appreciable, given by

$$R_{1\hat{\perp}} = (4/45)(\gamma_I \beta e)^2 \left(\frac{\mu_o}{4\pi}\right)^2 {r_{IS}}^{-6} [2 -$$
$$P_2(\cos\theta_{\hat{z}})](2[g_e^{(\pm 1/2)}]2P^o_{1/2} J_{\hat{\imath}}(\omega_I + \omega_{1/2})) \quad (2b)$$

where $\omega_{1/2}$ is the doublet splitting, which equals zero in the absence of a Zeeman field. The angular function, $[2 - P_2(\cos\theta_{\hat{z}})]$, which describes the sum of the $\hat{x}$ and $\hat{y}$ contributions, is preferentially directed in the plane.

The Electron *g*-Factor. The calculation of the magnetic dipolar field generated by the unpaired electrons at the positions of the various nuclear spins requires effective magnetic moments which may in turn be related to electronic *g*-values. These moments differ from those used to calculate magnetic susceptibilities in that they do not contain contributions arising from Zeeman mixing of zero-field states of different energies. The large zero-field splitting in $Co^{II}(acac)_2(H_2O)_2$ may be viewed as a consequence of the large first-order spin−orbit splitting in the $^4T_{1g}$ ground multiplet of octahedral Co(II). Using parameters of $\Delta = 9300$ cm^{-1} and $\zeta = 435$ cm^{-1} (ref 32), together with an effective axial splitting $\delta = -550$ cm^{-1}, we previously obtained[27] for the axially symmetric tetragonal case ($E = 0$) values of $g_{\|} = 2.43$ and $g_{\perp} = 4.99$ for the lowest ($|M_J| = {}^1/_2$) doublet. These values assumed an effective $S' = {}^1/_2$ if referenced to the true $S = {}^3/_2$ as we do here, $g_{\perp} = {}^{4.99}/_2 = 2.50$, indicating that use of an isotropic *g* of approximately 2.45−2.50 is justifiable for this lower energy doublet. For the upper $|M_J| = {}^3/_2$ doublet, we similarly obtained $g_{\|} = 5.29$ if referenced to $S' = {}^1/_2$, or $g_{\|} = {}^{5.29}/_3 = 1.76$ if referenced to the true $S = {}^3/_2$. In this axial limit, $g_{\perp} = 0$ for the $|M_J| = {}^3/_2$ doublet with Zeeman splittings arising in second order from off-diagonal mixings with the lower energy $|M_J| = {}^1/_2$ doublet. However because the axial zero-field splitting is very large, approximately 165.4 cm^{-1}, corresponding to a *D* parameter of $165/2 = 82.5$ cm^{-1}, it is quite justifiable to neglect Zeeman matrix elements between the doublets, so for simplicity we may assume an isotropic *g* of approximately 1.80 for the upper Kramers doublet. We have also reported[27] *g*-values computed for the orthorhombic case ($E \neq 0$), but the changes from the axial case are too small to consider here.

Summarizing these results, for the calculation of the strength of the local magnetic dipolar field generated by the unpaired electrons, we use isotropic *g*-values of $g_e^{(\pm 1/2)} = 2.45$ and $g_e^{(\pm 3/2)} = 1.80$ together with spin matrix elements appropriate to $S = {}^3/_2$ to compute magnetic moments. This approach differs from that normally used in the analysis of high-spin Co(II) ESR spectra, where the isolated Kramers doublets are treated as effective spin-$^1/_2$ systems. In that description, the *g*-factors are highly anisotropic and are very different for the $m_S = \pm^3/_2$ and $m_S = \pm^1/_2$ doublets; typically, $g_{\perp} \approx 4$, $g_{\|} \approx 2$ for $|\pm^1/_2\rangle$ and $g_{\perp} \approx 0$, $g_{\|} \approx 6$ for $|\pm^3/_2\rangle$.

Influence of the Boltzman Population Factors. The ZFS of Co(II) is large, comparable to *kT* at 300 K, and thus, the Boltzmann populations $P^o_{m_S}$ are outside the high-temperature limit. For $2D \approx 160$ cm^{-1}, the fractional populations of the $m_S = \pm^3/_2$ doublet are 0.46 that of the $m_S = \pm^1/_2$ doublet. The spin populations enter eq 2a,b as products of the form $\tau'_{S,m_S} = P^o_{m_S} \tau_{S,m_S}$ (this is true because the denominators of the significant spectral density functions very nearly equal unity), and it is these products which are determined by fits to theory. In the following discussion, we refer to the quantities τ'_{S,m_S} as electron spin relaxation times, using a prime to indicate the presence of the Boltzmann factor.

Experimental Section

The orange-red complex $Co^{II}(acac)_2(H_2O)_2$ was synthesized by the method of Ellern and Ragsdale.[32] The ligand 2,4-pentanedione (acac) was added slowly to aqueous NaOH (equal molar quantity as 2,4-pentanedione) with the temperature maintained <40 °C. The yellow-colored solution was added dropwise to an aqueous solution of $CoCl_2 \cdot (H_2O)_6$, where the Co(II) salt was one-half the final molar concentration of 2,3-pentanedione. The resulting precipitate was filtered and washed with water. The solid was then dissolved in a hot mixture of 95% EtOH and $CHCl_3$. The red solution was slowly cooled to room temperature in ice. The precipitate was filtered under vacuum, washed with 95% EtOH, and air-dried. Characterization by IR[33] and magnetic moment[34,35] ($\mu = 5.11$ μ_B) measurements agreed with literature.

The *inter*molecular R_1 relaxation rates were measured as a function of magnetic field strength for the solvent protons in a 20 mM solution of the complex in 1,4 dioxane to which 0.5% v/v ^2H_2O had been added. The solution and a diamagnetic blank were deoxygenated using five freeze−pump−thaw cycles and sealed under vacuum. R_1 measurements at Zeeman field strengths <2 T were made on a home-built, variable field NMR spectrometer specialized for relaxation measurements.[24,36] All R_1 values were measured using the phase-shifted triplet sequence, $(\pi)-[\tau_d-(\pi/2)_0-\tau_{tr}-(\pi)_\pi-\tau_{tr}-(\pi/2)_0]_n$, in which the magnetization decay following the initial inverting pulse is sampled periodically at intervals τ_d by a pulse triplet $[\tau_d-(\pi/2)_0-\tau_{tr}-(\pi)_\pi-\tau_{tr}-(\pi/2)_0]_n$. This sequence provides a rapid and accurate R_{1p} measurement. Using this sequence chemical shift information is suppressed. T_1 measurements at 4.7, 7.0, and 8.6 T were obtained using commercial high-resolution NMR spectrometers by means of the inversion−recovery technique.

The measurement of the axial/equatorial R_{1p} ratio of the complex in aqueous solution requires the measurement of both the water proton R_1 (near-axial) and the acac-methyl proton R_1 (near-equatorial). These measurements were made at 10.2 MHz, a field strength which corresponds approximately to the ZFS

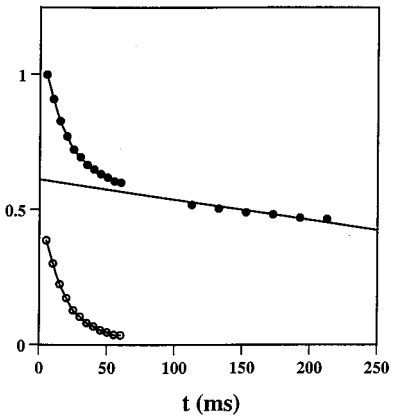

Figure 3. T_1 decay of the composite methyl/methine/water proton signal of 20 mM $Co^{II}(acac)_2(H_2O)_2$, dissolved in 99.96% ^2H_2O (solid circles). Also shown is the decay of the acac-methyl proton signal after subtraction of the water baseline (open circles). The acac-methine protons were partially deuterated by chemical exchange with the solvent and accounted for about 3% of the signal at $t = 0$. The slow component of the decay was due to residual water protons, the fast component due to acac-methyl protons. Measurements were conducted at a Zeeman field strength of 0.24 T, 20 °C.

limit. The water proton R_{1p} was measured in 15 mM aqueous solution. The methyl protons were measured in a saturated solution prepared in ^2H_2O (99.96% ^2H). The sample temperature 20 °C was controlled by a stream of dry nitrogen and monitored by a calibrated thermistor placed in a dummy sample tube.

Results

ZFS Limit Axial/Equatorial R_{1p} Ratio. A 200 MHz high-resolution NMR spectrum of $Co^{II}(acac)_2(^2H_2O)_2$ in ^2H_2O exhibited three peaks arising from the methyl and methine protons and from residual protonated solvent, with integrated intensities of 1.0:0.1:1.2. The ratio of methyl/methine peak integrals was larger than the expected value of 6:1 due to exchange of methine protons with deuterium in the solvent. The ZFS limit acac-methyl proton R_1 was measured at 10.2 MHz (0.24 T) using the phase-shifted triplet sequence (see above), which samples a composite signal of methyl, methine, and solvent protons on top of a spin echo. The separation of the water and methyl proton decay was carried out as described previously,[24] ignoring the methine contribution (which was about 50% deuterated). The decay was highly nonexponential, the methyl protons relaxing approximately 20 times faster than water protons (Figure 3), so the water and methyl components were easily separated. The acac-methyl proton decay (Figure 4) gave $R_{1p}(CH_3) = 45\ s^{-1}$.

The water proton R_1, measured separately at 10.2 MHz for a 15 mM solution of $Co^{II}(acac)_2(H_2O)_2$ in protonated H_2O, was $1.60 \pm 0.01\ s^{-1}$. The measured *intra*molecular R_{1p}, after correcting for the diamagnetic background ($0.321 \pm 0.007\ s^{-1}$) and the *inter*molecular paramagnetic contribution ($R_{1p}(inter) = 0.45\ s^{-1}$), was $R_{1p}(intra) = 0.83\ s^{-1}$. $R_{1p}(inter)$ was measured in a separate experiment using the dioxane proton resonance of a sample prepared in dioxane, a noncoordinating solvent.

R_{1m} ($\equiv T_{1m}^{-1}$) for the bound water protons was calculated from $R_{1p}(intra)$ using the Luz−Meiboom equation[37]

$$R_{1m}(intra) = f_m(T_{1m} + \tau_m)^{-1}$$

where f_m is the fraction (bound/free) of solvent protons and τ_m is the mean residence time of water bound in the complex. Variable temperature measurements of R_{1p} (not shown) demonstrated that chemical exchange is rapid, $\tau_m \ll T_{1m}$, giving $R_{1m}(H_2O) = 1562 \pm 50\ s^{-1}$ at 10.2 MHz, 20 °C.

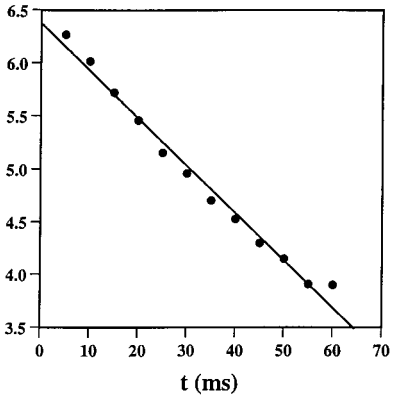

Figure 4. T_1 decay of the methyl proton decay, taken from the data of Figure 3, after subtraction of the slowly decaying component.

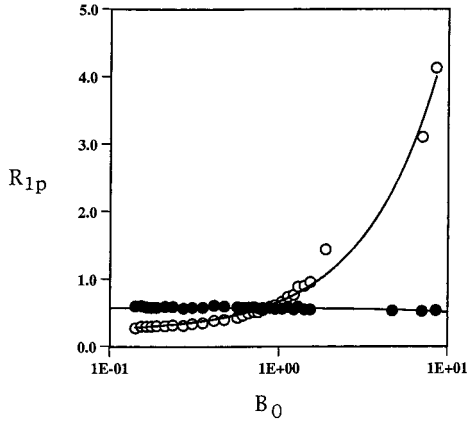

Figure 5. T_1 magnetic field dispersion profile (20 °C) of the solvent dioxane protons in a solution of 20 mM $Co^{II}(acac)_2(H_2O)_2$, prepared in a dioxane solvent which contained 0.5% (v/v) water (solid circles). Open circles show a previously reported[10] T_1 fdp of an analogous sample containing $Ni^{II}(acac)_2(H_2O)_2$, prepared in the same solvent and measured at the same temperature.

The axial/equatorial R_{1p} ratio, uncorrected for the difference in interspin distance r_{IS}, was 34.7 ± 1.5. This value was corrected for the difference in axial and equatorial I−S interspin distances using results from X-ray[38] and neutron diffraction[39] studies. The Co−O (water) distance in $Co(acac)_2(H_2O)_2$ is 2.22 ± 0.02 Å. Using the standard O−H bond distance in water (0.96 Å) and a cock angle of 14° between the plane of the water molecule and the Co−O axis gives a Co−H distance of 2.93 ± 0.06 Å (Co to water hydrogens). Cock angles in the range 14°−17° have been measured from neutron diffraction studies[39] of aquated divalent transition metal cations. From the X-ray crystal structure of the complex, the average Co−C distance for the methyl carbons is 4.29 ± 0.03 Å. Assuming tetrahedral bond angles, the average Co−H distance (calculated as $(\langle r^{-6}\rangle)^6$) to the methyl protons is 4.56 ± 0.03 Å. The correction factor, r_{ax}^{-6}/r_{eq}^{-6}, is 13.1, giving a distance-corrected axial/equatorial R_{1p} ratio, $\rho_{exp} = 2.7 \pm 0.4$.

Comparison of $S = 1$ and $S = {}^3/_2$ T_1 Field Dispersion Profiles. An experiment was also conducted to determine whether the ZFS rhombicity-induced dispersive feature that is characteristic of orthorhombic $S = 1$ spin systems (see above) is likewise present in the T_1 magnetic field dispersion profile of analogous $S = {}^3/_2$ spin systems. An experimental example[10] of this feature is shown in Figure 5 (open circles) for the $S = 1$ complex $Ni^{II}(acac)_2(H_2O)_2$. An analogous experiment was conducted using the $S = {}^3/_2$ complex, $Co^{II}(acac)_2(H_2O)_2$, with

results shown as solid circles in the figure. In both experiments, the NMR samples were prepared in a dioxane solvent containing 0.5% (v/v) water. The magnetic field dispersion profiles in Figure 5 were measured for the *inter*molecular R_{1p} of the dioxane solvent protons. Use of *inter*molecular R_{1p} data provides a direct comparison between the two spin systems in which only the spin dynamics, not the molecular structure variables θ and r_{IS}, play a role. The concept that dioxane does not enter the metal coordination sphere was tested by comparing the UV−vis spectra of samples containing $M^{II}(acac)_2(H_2O)_2$ (M = Ni-(II) and Co(II)) dissolved at equal concentrations in water and in a dioxane solvent containing 0.5% water. The UV−vis spectra of samples prepared in the two solvents were essentially identical, indicating that dioxane remains outside the metal coordination sphere.

Figure 5 shows the T_1 magnetic field dispersion profile (fdp) for the dioxane protons of these two systems over the range 0.15−8.6 T. The large ZFS rhombicity-induced dispersive feature in the fdp of the $S = 1$ complex is absent for the $S = {}^3/_2$ complex. This difference in behavior is expected theoretically (see below) and results from the fact that ZFS rhombicity splits the non-Kramers $|\pm 1\rangle$ doublet of $S = 1$ but not the Kramers doublets of $S = {}^3/_2$. For $S = {}^3/_2$, ZFS rhombicity produces a very small downward dispersive feature which is described below.

Results of Simulations

Axial/Equatorial R_{1p} Ratio. The slow-reorientation theory (eq 2) was used to fit the experimentally determined axial/equatorial R_{1p} ratio. All distances and angles required by the simulations were held fixed at the values determined by the X-ray and neutron diffraction studies as described above. The theory depends on the following electron spin parameters: D, E, and the relaxation times $\tau_{S,\pm 1/2}$ and $\tau_{S,\pm 3/2}$, of the two Kramers doublets. The value of the *inter*doublet splitting $2D$ for $Co^{II}(acac)_2(H_2O)_2$ has been estimated to be 160 cm^{-1} from a fit to temperature-dependent magnetic susceptibility data.[27] For a splitting of this magnitude, the simulations are almost independent of the magnitude of D apart from effects on the Boltzmann populations because $J(2\omega_D) \approx 0$. The effect of the ZFS rhombicity E was explored in test calculations, and this parameter likewise was found to exert very little influence on the low field limiting value of R_{1p}. The influence of E for $S = {}^3/_2$ is very different than for integer spin cases, where ZFS rhombicity splits the non-Kramers doublets, forcing a Cartesian polarization on the spin eigenfunctions and, in consequence, profoundly depressing the ZFS-limit NMR-PRE (see below). Taking the molecular structure parameters as known, the calculated R_{1p} is almost entirely determined by the level-specific electron spin relaxation times within the two spin manifolds. Thus, the calculation involves two measured quantities (R_{1p} for the water protons and the acac-methyl protons) and two parameters ($\tau'_{S,\pm 1/2}$ and $\tau'_{S,\pm 3/2}$). Agreement between experiment and calculation was found for $\tau'_{S,\pm 3/2} = 1.5 \pm 0.2$ ps and $\tau'_{S,\pm 1/2} = 0.2 \pm 0.2$ ps. The calculated ZFS limit R_{1p} ratio, corrected for the difference in interspin distance, was $\rho_{exp} = 2.7 \pm 0.4$ (Table 1).

Calculation of the Intermolecular R_{1p}. The T_1 fdp of the dioxane solvent protons, shown in Figure 5, was simulated using the slow-reorientation simulation techniques contained within the computer program RotJmpDyn.f,[10] which describe R_{1p}(*inter*) in the ZFS limit and intermediate regimes. Results of the simulations are shown in Figure 6. The simulatons depended very little on the ZFS parameters D and E for $D > 25$ cm^{-1}, as was likewise true for the calculations for R_{1p}(*intra*) described above. There was, however, a strong dependence on the electron spin relaxation times, for which the values in Table 1 were used; these values were derived from R_{1p}(*intra*) measurements of the water and acac-methyl protons as described above.

TABLE 1: Calculated and Experimental Axial/Equatorial R_{1p} Ratios and Experimental (ρ_{exp}), Zeeman Limit (ρ_{Zeem}), and ZFS-Limit (ρ_{ZFS}) Axial/Equatorial Ratios[a]

complex	ρ_{exp}	ρ_{ZFS} (SR)	ρ_{ZFS} (SD)	ρ_{Zeem}
$Co^{II}(acac)_2(H_2O)_2$[b]	2.7 ± 0.4	2.7		1
$Ni^{II}(acac)_2(H_2O)_2$[c]	2.2 ± 0.3	4.0	2.4	1

[a] The ZFS limit ratios were calculated from slow reorientation (SR) theory (eq 1 of the text) and, for the Ni(II) complex, by spin dynamics (SD) simulation. [b] Calculations assumed $D = 80$ cm^{-1}, $E = 0$, $\tau_S^{(\pm 1/2)} = 0.2$ ps, and $\tau_S^{(\pm 3/2)} = 2.0$ ps (the calculated ratio was nearly independent of D and E). [c] Experimental results taken from ref 24; ZFS-limit calculations assumed $D = 3.2$ cm^{-1}, $E = 0.52$ cm^{-1}, $\tau'_S = 19$ ps, and $\tau_R^{(2)} = 77$ ps.

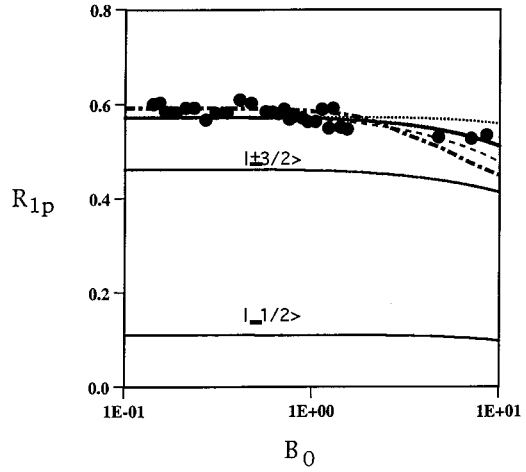

Figure 6. Simulations of the $Co^{II}(acac)_2(H_2O)_2$ fdp shown in Figure 5. Calculations (except bold dash−dot) were based on eq 1 of the text with the parameter values shown in Table 1. The calculations assumed a ZFS parameter $D = 80$ cm^{-1} but were essentially insensitive to variations in D for $D > 25$ cm^{-1}. Results are shown for three values of E: $E = 0$ (dashed); $E = 7$ cm^{-1}(solid line); $E = 15$ cm^{-1} (dashed). R_{1p} contributions of the $m_S = \pm {}^3/_2$ and $m_S = \pm {}^1/_2$ doublets are indicated. The bold dash−dot curve assumes equal electron spin relaxation times in the $m_S = \pm {}^1/_2$ and $m_S = \pm {}^3/_2$ doublet manifolds.

The simulation of R_{1p}(*inter*) also depends on an I−S "distance of closest approach" parameter, d_c, rather than upon r_{IS}. The calculated R_{1p}(*inter*) was in agreement with experiment when $d_c = 3.4$ Å. A molecular dynamics simulation of d_c, carried out using the commercial program Cerius[2] (Biosym/MSI, Inc.), suggested a slightly larger value for the physical distance of closest approach, $d_c = 3.6 \pm 0.2$ Å (Figure 7). This difference probably results from the nonspherical shape of the solute, coupled with the fact that the axial/equatorial R_{1p} ratio is >1.[40] R_{1p}(*inter*) also depends in principle on the mutual diffusion coefficient of the solvent and solute, but in the present system electron spin relaxation is rapid with respect to diffusional motion, which thus has negligible influence on the calculation.

The simulated (bold solid line) and experimental (symbol) R_{1p}(*inter*) profiles for $Co^{II}(acac)_2(H_2O)_2$, compared in Figure 6, are in good agreement. The fact that the R_{1p}(*inter*) profile was accurately simulated using electron spin relaxation times derived from a separate experiment using R_{1p}(*intra*) data for the water and acac-CH_3 resonances provides an internal check on the consistency of the overall analysis.

An assumption that the electron spin relaxation times in the two doublet manifolds are approximately equal, i.e., $\tau_{S,\pm 1/2} \approx$

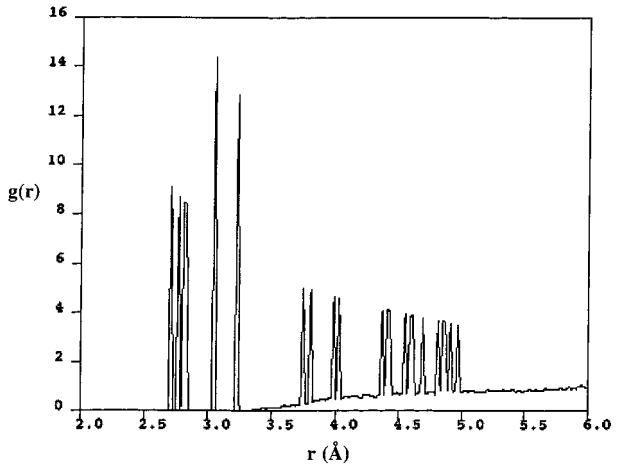

Figure 7. Co(II)−proton radial distribution function $g(r)$ of a solution of $Co^{II}(acac)_2(H_2O)_2$ in dioxane. Results were generated by a molecular dynamics simulation using the simulations software package of Cerius[2] (Biosym/MSI, Inc.). Periodic boundary conditions were assumed with a unit cell containing one solute molecule plus 36 dioxanes. The solute was constrained to be rigid with a Co−C−O backbone taken from the X-ray structure. The sharp peaks correspond to *intra*molecular distances from Co(II) to water, methine, and methyl protons, while Co−H distances to the dioxane constitute the continuous background. A *T*-damping algorithm was used to simulate constant temperature conditions at $T = 20$ °C. The simulation employed 1 fs time steps and a total duration of 20 ps.

$\tau_{S,\pm 3/2}$, did not produce high-quality fits to the high-field data. Figure 6 (bold dash−dot line) shows a simulated fdp which assumes that $\tau_{S,\pm 1/2} = \tau_{S,\pm 3/2}$ and that these quantities have the magnitude required to give the measured R_{1p} at $B_0 = 0$. This simulation does not fit the data well in the high-field region. This is because the $m_S = \pm^1/_2$ contribution to R_{1p} originates largely in the transverse ($R_{1\perp}$) term, which disperses away when $\omega_{\pm 1/2}\ \tau_{S,\pm 1/2} \geq 1$ ($\omega_{\pm 1/2}$ is the *intra*doublet splitting). If the contribution of the $|\pm^1/_2\rangle$ manifold were important (as is required if $\tau_{S,\pm 1/2} = \tau_{S,\pm 3/2}$), the fdp would exhibit a substantial downward dispersion at Zeeman field strengths of several tesla. The absence of such a feature in the data thus supports the conclusion, reached above on the basis of the measured ZFS limit axial/equatorial R_{1p} ratio, that $\tau_{S,\pm 1/2} \ll \tau_{S,\pm 3/2}$.

The very slight (<5%) downward dispersion in the experimental fdp of Figure 6 might result from the $|\pm^1/_2\rangle$ contribution with $\tau_{S,\pm 1/2} \ll \tau_{S,\pm 3/2}$, although this feature seems more likely to result from the effects of ZFS rhombicity, which mixes the $m_S = \pm^1/_2$ and $\pm^3/_2$ levels, thus bringing $m_S = \pm^1/_2$ character into the zero-order $m_S = \pm^3/_2$ spin eigenstates. As a result, the $|\pm^3/_2\rangle$ doublet, which provides the bulk of the NMR relaxation efficiency, exhibits an sdf-type dispersion due to the small rhombicity-induced $|\pm^1/_2\rangle$ component of the $|\pm^3/_2\rangle$ wave function. This phenomenon is shown in the simulations of Figure 6, where increasing ZFS rhombicity introduces a downward dispersion into the fdp without influencing the ZFS-limit magnitude of R_{1p}. An accurate fit of the data occurs for $E/D \approx 0.1$, using the $\tau_{S,\pm 1/2}$ and $\tau_{S,\pm 3/2}$ values given in the table.

Discussion

Table 1 compares a series of theoretical and experimental axial/equatorial R_{1p} ratios for the $S = {}^3/_2$ complex, $Co^{II}(acac)_2(H_2O)_2$, and the $S = 1$ complex, $Ni^{II}(acac)_2(H_2O)_2$. For $S = {}^3/_2$, as was previously found[24] for $S = 1$, the quantity $\rho_{exp} = 2.7 \pm 0.4$ is significantly greater than the Zeeman limit value of unity, thus confirming a central prediction of ZFS-limit NMR-PRE theory.

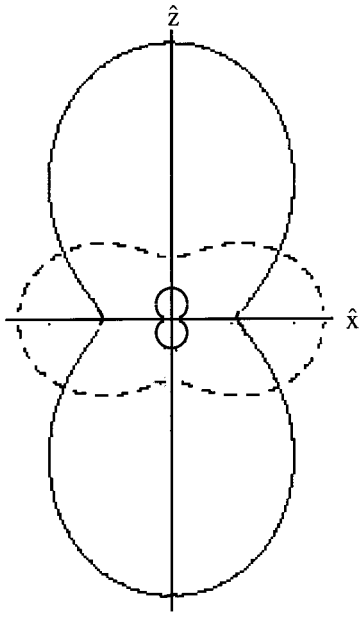

Figure 8. Polar plots of the functions $(m_S)^2[1 + P_2(\cos\theta_{\hat{z}})]$ for $m_S = \pm^3/_2$ (outer solid line) and $m_S = \pm^1/_2$ (inner solid line). Also shown is a polar plot of the function $|\langle +^1/_2|S_{\hat{x}}|-^1/_2\rangle|^2[2 - P_2(\cos\theta_{\hat{z}})]$ (dashed line).

The magnetic field dispersion profile for $Co^{II}(acac)_2(H_2O)_2$ was nearly field-independent below 8.6 T and lacked the profound rising dispersive feature that is characteristic of $S = 1$ orthorhombic Ni(II) complexes. This behavior likewise confirms theoretical prediction.

Physical Origin of the Molecular Frame Anisotropy in R_{1p}. A physical model of the slow reorientation ZFS-limit relaxation mechanism, for which eq 2 supplies the mathematical description, is given in ref 8. We briefly summarize the physical picture here. The NMR-PRE results from additive contributions, with $R_{1\hat{r}}$ ($\hat{r} = \hat{x}, \hat{y}, \hat{z}$) arising from the molecular frame Cartesian components of the electron spin magnetic moment, $\langle\mu_{\hat{x}}\rangle = g_e\beta_e\langle S_{\hat{x}}\rangle$. $R_{1\hat{x}}$ can be viewed as resulting, in a semiclassical picture, from the local field at I due to a sum of oscillating electron spin dipoles located at the origin and directed along $\hat{x}$. Each dipole of the sum corresponds to a nonvanishing matrix element, $\langle\mu|\mu_{\hat{x}}|\nu\rangle$, of $\langle\mu_{\hat{x}}\rangle$ oscillating at the $\{\mu \rightarrow \nu\}$ transition frequency, $\omega_{\mu,\nu}$. R_{1p} is proportional to the square of the local dipolar field times the dipolar power density at the nuclear Larmor frequency, ω_I (i.e., only resonant coupling contributes to the process of energy transfer). The power density at ω_I produced by $\langle\mu|\mu_{\hat{x}}|\nu\rangle$ is proportional to the spectral density function, $J(\omega_{\mu,\nu} + \omega_I)$, and the squared local dipolar field due to $\langle\mu_{\hat{r}}\rangle$ varies spatially as the function $r_{IS}^{-6}[1 + P_2(\cos\theta_{\hat{r}})]$. In the special case of a cylindrical ZFS tensor (eq 2), the $\hat{x}$ and $\hat{y}$ contributions to R_{1p} have been combined in the spatial function, $r_{IS}^{-6}[2 - P_2(\cos\theta_{\hat{z}})]$.

Polar plots of the angular functions $(1 + P_2(\cos\theta_{\hat{z}}))$ and $(2 - P_2(\cos\theta_{\hat{z}}))$, weighted by the squared matrix elements $|\langle S_{\hat{z}(\hat{x})}\rangle|^2$, are shown in Figure 8. All of the terms contributing to $R_{1\hat{z}}$ vary spatially as the function $(1 + P_2(\cos\theta_{\hat{z}}))$ and are 4-fold larger at axial nuclear positions than at equatorial positions. $R_{1\hat{x}}$ varies spatially as the function $(2 - P_2(\cos\theta_{\hat{z}}))$ and is 2.5 times larger at equatorial positions than at axial positions.

We consider the relative magnitudes of the relaxation pathways of $R_{1\perp}$ and $R_{1\hat{z}}$ within the Kramers doublets of Co(II). In eq 1b, the magnitudes of the $R_{1\hat{r}}$ depend on the quantities $P_\alpha^o\, g_e^2|\langle S_{\hat{r}}\rangle|^2 J(\omega_{\alpha,\beta})$ where $J(\omega_{\alpha,\beta})$ are spectral density functions evaluated at the transition frequencies of the nonvanishing

matrix elements of $\langle S_{\hat{r}}\rangle$. Within the $m_S = \pm^3/_2$ doublet, $R_{1\hat{z}}$ is significant but $R_{1\hat{\perp}}$ is not, since the transverse spin matrix elements $\langle S_{\hat{x}(\hat{y})}\rangle$ vanish for all except the 1Q transitions, for which the transition frequencies, $2\omega_D$, are very high and the spectral density functions, $J(2\omega_D)$, are very small. Within the $|\pm^3/_2\rangle$ doublet manifold, $\langle S_{\hat{z}}\rangle$ is diagonal and contributes relaxation efficiency proportional to

$$R_{1\hat{z}} \propto P^{o}_{3/2}|\langle S_{\hat{z}}\rangle|^2 J(0)|$$
$$= P^{o}_{3/2}(m_S{}^2)\,\tau_{S,\pm 3/2}$$

$R_{1\hat{z}}(\pm^3/_2)$ is relatively large both because of the large value of $|\langle S_{\hat{z}}\rangle|^2$, and because, in the case of Co(II), $\tau_{S,\pm 3/2}$ is relatively long. $R_{1\hat{\perp}}(\pm^3/_2)$ is negligible because $J(2\omega_D) \approx 0$.

The relaxation pathway within the $|\pm^1/_2\rangle$ Kramers doublet is rather different. Here the contribution of $R_{1\hat{z}}$ is negligible due to the combined effects of small $m_S{}^2$ and short $\tau_{S,\pm 1/2}$. The transverse contribution is not negligible, however. $R_{1\hat{\perp}}(\pm^1/_2)$ has a significant zero frequency contribution due to the $\{+^1/_2 \leftrightarrow -^1/_2\}$ 1Q transition, for which the squared matrix element, $|\langle +^1/_2|S_{\hat{x}(\hat{y})}|-^1/_2\rangle|^2$, equals unity. The dashed curve in Figure 8 shows the weighted angular function, $|\langle S_{\hat{x}(\hat{y})}\rangle|^2[2 - P_2(\cos\theta_{\hat{z}})]$, which appears in the contributions to $R_{1\hat{\perp}}$. It is this contribution that causes the calculated axial/equatorial R_{1p} ratio to be less than 4 (the value for $R_{1\hat{z}}$).

Figure 8 shows polar plots of the weighted functions $|\langle\mu|S_{\hat{r}}|\nu\rangle|^2 J_{\hat{r}}(\omega_{\mu,\nu})$ for the terms of eq 1b that contribute significantly to R_{1p}. These functions are expected to provide a relative estimate of the level-specific relaxation efficiencies for the $S = {}^3/_2$ ion, Cr(III), where the ZFS splitting is relatively small and the populations, *g*-values, and electron spin relaxation times are approximately equal for both Kramers doublets. For Cr(III), the ZFS-limit axial/equatorial R_{1p} ratio is expected to be approximately $\rho = ({}^8/_5)$ under slow reorientation conditions, as opposed to the value $\rho = 4$ for $S = 1$ under equivalent assumptions (the principal assumption being that the *inter*doublet transitions do not contribute significantly to $R_{1\hat{\perp}}$ for either spin value).

For Co(II), the situation is quite different, as described above. The relaxation efficiencies are approximately described by the polar plots of Figure 9, which shows the functions

$$f_{\hat{z}}(\pm^3/_2) = [g_e^{(\pm 3/2)}]^2(1 + P_2(\cos\theta_{\hat{z}}))P^{o}_{\pm 3/2}|\langle S_{\hat{z}}\rangle|^2\tau_{S,\pm 3/2} \quad (3a)$$

$$f_{\hat{\perp}}(\pm^1/_2) = [g_e^{(\pm 1/2)}]^2(2 - P_2(\cos\theta_{\hat{z}}))P^{o}_{\pm 1/2}|\langle S_{\hat{x}}\rangle|^2\tau_{S,\pm 1/2} \quad (3b)$$

These plots, which assume $P^{o}_{1/2} = P^{o}_{3/2}$, are proportional to the relaxation efficiency at constant r_{IS}. Clearly the bulk of the relaxation efficiency is produced by $R_{1\hat{z}}(\pm^3/_2)$ with negligible contribution from $R_{1\hat{z}}(\pm^1/_2)$. $R_{1\hat{\perp}}(\pm^1/_2)$ produces a relatively small but significant relaxation contribution which reduces the axial/equatorial R_{1p} ratio from the value of $\rho = 4$ produced by $R_{1\hat{z}}$ down to the observed value, $\rho_{exp} = 2.7$.

Difference in Electron Spin Relaxation within the $|\pm^1/_2\rangle$ and $|\pm^3/_2\rangle$ Doublets. Electron spin relaxation rates within the $|\pm^1/_2\rangle$ and $|\pm^3/_2\rangle$ Kramers doublets differ by about an order of magnitude. In this section, we provide a possible explanation for this difference. Electron spin relaxation for $S \geq 1$ is caused by stochastic fluctuations in the ZFS tensor, which result, on the molecular level, from collisional and vibrational distortions of the metal coordination sphere as well as from reorientation of the static ZFS tensor. Reorientationally induced electron spin relaxation is negligible for Co(II) because $\tau_S \ll \tau_R^{(2)}$.

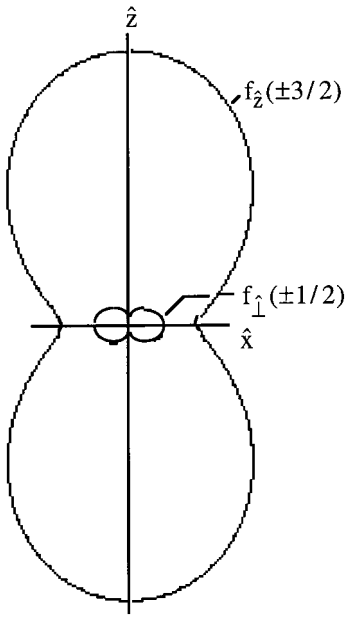

Figure 9. Polar plots of the functions $f_{\hat{z}}(\pm^3/_2)$ and $f_{\hat{\perp}}(\pm^1/_2)$ as defined in eq 3. These functions are proportional to the paramagnetic NMR relaxation efficiency.

For $S = {}^3/_2$, the total electron spin Hamiltonian is quadratic, a sum of static and stochastic terms of the form

$$H_S = H_S^{(o)} + H'_S(t)$$

$$H_S^{(o)} = D(S_{\hat{z}}{}^2 - S(S+1)/3) + E(S_{\hat{x}}{}^2 - S_{\hat{y}}{}^2)$$

$$H'_S(t) = \sum_{q=-2}^{+2} a_q^{(2)}(t)\,{}^{(2)}_{Sq}$$

The spin operators of $H'_S(t)$ are written in spherical tensor form. $H'_S(t)$ induces relaxation transitions between the spin eigenfunctions of $H_S^{(o)}$.

The terms of $H'_S(t)$ with $q = \pm 1, \pm 2$ induce transitions between levels for which $\Delta m_S = \pm 1, \pm 2$, respectively. Thus the $q = \pm 1$ terms induce the following transitions: $\{|+^3/_2\rangle \leftrightarrow |+^1/_2\}$, $\{|+^1/_2\rangle \leftrightarrow |-^1/_2\}$, and $\{|-^1/_2\rangle \leftrightarrow |-^3/_2\}$. The terms with $q = \pm 2$ induce the transitions $\{|+^3/_2\rangle \leftrightarrow |-^1/_2\}$ and $\{|+^1/_2\rangle \leftrightarrow |-^3/_2\}$. Since $H'_S(t)$ contains only quadratic terms (higher order terms vanish for $S = {}^3/_2$), no transitions are allowed within the $|\pm^3/_2\rangle$ Kramers doublet to lowest (2nd) order in relaxation theory.

The terms of $H'_S(t)$ which induce relaxation transitions, correspond to specific distortional symmetries of the static ZFS tensor. The terms with $q = \pm 1$ can be written in linear combinations as Cartesian functions which transform as $\hat{x}\hat{z}$ and $\hat{y}\hat{z}$. These terms describe, to first order in the displacements, rotational motions of the ZFS tensor in which the $\hat{z}$-principal axis rotates toward the $\hat{x}(\hat{y})$ axis as shown in Figure 10a. The terms with $q = \pm 2$ can be written as Cartesian functions which transform as $\hat{x}\hat{y}$ and $\hat{x}^2 - \hat{y}^2$. The term that transforms as $\hat{x}\hat{y}$ describes a rotation of the $\hat{x}$- and $\hat{y}$-principal axes about $\hat{z}$ (Figure 10b). The $\hat{x}\hat{z}$ and $\hat{y}\hat{z}$ terms induce spin transitions with $\Delta m_S = \pm 1$, and $\hat{x}\hat{y}$ induces transitions with $\Delta m_S = \pm 2$. The remaining terms correspond to distortions of the ZFS tensor that transform as $\hat{z}^2$ ($q = 0$) and $\hat{x}^2 - \hat{y}^2$ ($q = \pm 2$), which do not induce spin transitions.

The *inter*doublet transition probabilities depend on the ZFS power density (i.e., that of $H'_S(t)$ at the *inter*doublet transition frequency, which is of order 100 cm^{-1}, while transitions within

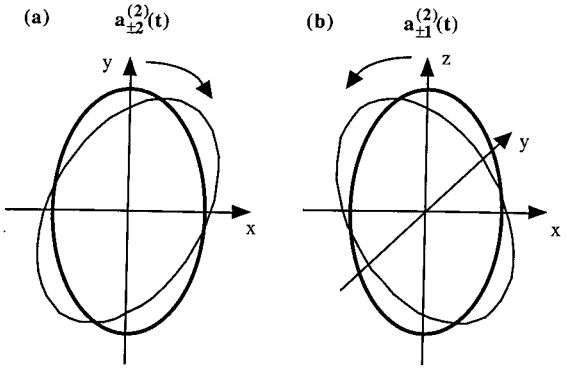

Figure 10. Schematic depiction of the effect on an orthorhombic ZFS tensor of a distortion of (a) *xy* symmetry and (b) *xz* symmetry. To first order, these distortions rotate the ZFS tensor about (a) the *z*-axis and (b) the *y*-axis without changing the ZFS principal values.

the $|\pm^1/_2\rangle$ Kramers doublet depend on the power density at or close to zero frequency. The Bloembergen−Morgan (B−M) relaxation theory[29] is based on collisionally induced zero-frequency centered fluctuations of the ZFS tensor. The NMR-PRE of many complexes is well described by the B−M mechanism using a collisional correlation time, τ_v, of about 3 ps. Collisional ZFS distortions of this kind have a power density which is centered below about 10 cm^{-1}, and thus they are ineffective in inducing transitions between the adjacent Kramers doublets of Co(II), for which frequencies of order 160 cm^{-1} are required. However, the B−M relaxation pathway is effective within the $|\pm^1/_2\rangle$ doublet where the transition frequency is, at most, a few wavenumbers. It is likely that relaxation within the $|\pm^1/_2\rangle$ doublet results from the B−M mechanism and is relatively efficient, while relaxation involving the $|\pm^3/_2\rangle$ levels, which cannot use the B−M pathway, is relatively inefficient. Because of the high frequencies of the allowed spin transitions involving the $|\pm^3/_2\rangle$ levels, the motions which induce these transitions will necessarily be vibrational (rather than distortional) in nature. (All relaxation transitions involving the $\pm^3/_2$ levels are also transitions for the $\pm^1/_2$ levels, but the converse is not true.)

This picture changes somewhat in the presence of static ZFS rhombicity, which mixes the $|\pm^3/_2\rangle$ eigenstates with the $|\pm^1/_2\rangle$ eigenstates, thereby giving the $|\pm^3/_2\rangle$ doublet a low-frequency relaxation pathway. It is possible that the bulk of the relaxation efficiency of the $|\pm^3/_2\rangle$ doublet arises from mixing of this kind.

Conclusions

The ZFS-limit axial/equatorial R_{1p} ratio has been measured for the $S = {}^3/_2$ complex, $Co^{II}(acac)_2(H_2O)_2$. The ratio was found to be significantly greater than the Zeeman limit value of unity, confirming a theoretical prediction that the ZFS-limit NMR-PRE depends on the orientation of the interspin I−S vector in the ZFS principal axis system.

The magnetic field dispersion profile for $Co^{II}(acac)_2(H_2O)_2$ was measured and found to lack the profound rising dispersive feature that is characteristic of $S = 1$ orthorhombic Ni(II) complexes. For $S = 1$ spin systems, this dispersive feature results from a splitting of the $|\pm 1\rangle$ non-Kramers doublet by the orthorhombic component of the ZFS tensor. The non-Kramers doublets of $S = {}^3/_2$ remain unsplit by ZFS interactions of any symmetry in the absence of an applied magnetic field, and thus, an analogous rising dispersive feature is predicted to be absent. The experiments thus confirm this theoretical prediction.

The NMR-PRE produced by the high-spin Co(II) was analyzed theoretically. For this ion, the electron spin relaxation times and *g*-values differ substantially in the $m_S = \pm^1/_2$ and $\pm^3/_2$ Kramers doublets, and the spin level populations are usually not well described by the high-temperature limit. The $m_S = \pm^1/_2$ Kramers doublet of $S = {}^3/_2$ provides a unique transverse contribution to the relaxation mechanism that has no counterpart in the relaxation mechanisms of integer spins.

Acknowledgment. This research was supported by the U.S. National Science Foundation in the form of a research grant, CHE-9423351.

References and Notes

(1) Sharp, R. R. *J. Chem. Phys.* **1990**, *93*, 6921.
(2) Bayburt, T.; Sharp, R. R. *J. Chem. Phys.* **1990**, *92*, 5892.
(3) Sharp, R. R. *J. Chem. Phys.* **1993**, *98*, 912.
(4) Sharp, R. R. *J. Magn. Reson.* **1992**, *100*, 491.
(5) Sharp, R. R. *J. Chem. Phys.* **1993**, *98*, 2507.
(6) Sharp, R. R. *J. Chem. Phys.* **1993**, *98*, 6092.
(7) Bovet, J.-M.; Sharp, R. R. *J. Chem. Phys.* **1993**, *99*, 18.
(8) Sharp, R. R.; Abernathy, S. M.; Lohr, L. L. *J. Chem. Phys.* **1997**, *107*, 7620.
(9) Abernathy, S. M.; Sharp, R. R. *J. Chem. Phys.* **1997**, *106*, 9032.
(10) Abernathy, S. M.; Sharp, R. R. *J. Phys. Chem. A* **1997**, *101*, 3692.
(11) Abernathy, S. M.; Miller, J. C.; Lohr L. L.; Sharp, R. R. *J. Chem. Phys.* **1998**, *109*, 4035.
(12) P.-O. Westlund has reviewed Swedish work prior to 1995 on the Stochastic Liouville/Pseudorotation Model in the following: Westlund, P.-O. In *Dynamics of Solutions and Fluid Mixtures by NMR*; Delpuech, J. J., Ed.; Wiley: New York, 1995; p 173.
(13) Larsson, T.; Westlund, P.-O.; Kowalewski, J.; Koenig, S. H. *J. Chem. Phys.* **1994**, *101*, 1116.
(14) Svoboda, J.; Nilsson, T.; Kowalewski, J.; Westlund, P.-O.; Larsson, P. T. *J. Magn. Reson., Ser. A* **1996**, *121*, 108.
(15) Westlund, P.-O. *Mol. Phys.* **1996**, *85*, 1165.
(16) Odelius, M.; Ribbing, C.; Kowalewski, J. *J. Chem. Phys.* **1996**, *103*, 1800; **1996**, *104*, 96.
(17) Strandberg, E.; Westlund, P.-O. *J. Magn. Reson., Ser. A* **1999**, *137*, 333.
(18) Westlund, P.-O. *J. Chem. Phys.* **1998**, *108*, 4945.
(19) Banci, L.; Bertini, I.; Luchinat, C. *Nuclear and Electron Relaxation*; VCH Publishers: Weinheim, Germany, 1991.
(20) Bertini, I.; Galas, O.; Luchinat, C.; Parigi, G. *J. Magn. Reson., Ser. A* **1995**, *113*, 151.
(21) Bertini, I.; Kowalewski, J.; Luchinat, C.; Nilsson T.; Parigi, G. *J. Chem. Phys.* **1999**, *111*, 5795.
(22) Solomon, I. *Phys. Rev.* **1955**, *99*, 555.
(23) Bloembergen, N. *J. Chem. Phys.* **1957**, *34*, 842.
(24) Miller, J. C.; Abernathy, S. M.; Sharp, R. R. *J. Phys. Chem.* **2000**, *104*, 4839.
(25) Fukui, H.; Miura, K.; Matsuda, H. *J. Magn. Reson.* **1999**, *88*, 311.
(26) Miller, J. C.; Lohr, L. L.; Sharp, R. R. *J. Magn. Reson.*, submitted for publication.
(27) Lohr, L. L.; Miller, J. C.; Sharp, R. R. *J. Chem. Phys*. **1999**, *111*, 10148.
(28) Miller, J. C.; Sharp, R. R. *J. Phys. Chem.* **2000**, *104*, 4839.
(29) Bloembergen, N.; Morgan, L. O. *J. Chem. Phys.* **1961**, *34*, 842.
(30) Abernathy, S. M.; Sharp, R. R. *J. Chem. Phys.* **1977**, *106*, 9032.
(31) Abragam, A. *The Principles of Nuclear Magnetism*; Oxford University Press: London, 1961; Chapter 8.
(32) Ellern, J. B.; Ragsdale, R. O. In *Inorganic Syntheses*; Jolly, W. L., Ed.; McGraw-Hill: New York, 1968; Vol. 11, pp 82−84.
(33) Holtzclaw, H. F.; Collman, J. P. *J. Am. Chem. Soc.* **1957**, *79*, 3318.
(34) Figgis, B. N.; Lewis, J. In *Modern Coordination Chemistry*; Lewis, J., Wilkins, R., Eds.; Interscience: New York, 1960; p 400.
(35) Cotton, F. A.; Wilkinson, G. *Advanced Inorganic Chemistry: A Comprehensive Text*, 4th ed.; Wiley and Sons: New York, 1980; p 771.
(36) Haddy, A. E.; Frasch, W. D.; Sharp, R. R. *Biochemistry* **1985**, *24*, 7926.
(37) Luz, Z.; Meiboom, S. *J Chem. Phys.* **1965**, *40*, 2686.
(38) Bullen, G. J. *Acta Crystallogr*. **1959** *12*, 703.
(39) Powell, D. H. *J. Phys.: Condens. Mater*. **1989**, *1*, 8721.
(40) The theoretical parameter d_c assumes the solute to be a diffusing hard sphere. In the ZFS limit, the $\hat{z}$-molecular axis is more strongly relaxing than are the $\hat{x}$- and $\hat{y}$-molecular axes, and the $\hat{z}$ direction is also more accessible to the solvent than is the equatorial plane. Thus, we expect the theoretical parameter d_c to be somewhat smaller than the physical distance of closest approach.